Available online at www.sciencedirect.com
SCIENCE DIRECT®
Nuclear Instruments and Methods in Physics Research A 536 (2005) 29–51
NUCLEAR INSTRUMENTS & METHODS IN PHYSICS RESEARCH Section A
www.elsevier.com/locate/nima

Electron detection with a dual-readout calorimeter

N. Akchurin[a], K. Carrell[a], J. Hauptman[b], H. Kim[a], H.P. Paar[c], A. Penzo[d], R. Thomas[a], R. Wigmans[a,*]

[a]*Department of Physics, Texas Tech University, Lubbock, Lubbock, TX 79409-1051, USA*
[b]*Iowa State University, Ames, USA*
[c]*University of California at San Diego, La Jolla, USA*
[d]*INFN Trieste, Italy*

Received 24 June 2004; accepted 29 June 2004
Available online 25 August 2004

Abstract

Electromagnetic shower development in a copper-based fiber calorimeter is studied by simultaneously measuring the scintillation light and the Cherenkov light generated in this process. We report on the energy resolution, the signal linearity and the dependence of the response function on the impact point and the angle of incidence.The electrons range in energy from 8 to 200 GeV. Differences observed between the results from the two types of signals are presented and interpreted.

Keywords: Sampling calorimetry; Optical fibers; Electromagnetic showers; Cherenkov light

1. Introduction

The detector discussed in this paper was primarily developed for the purpose of detecting *hadrons and hadron jets* with excellent precision. Traditionally, this goal is incompatible with the requirements of excellent electromagnetic calorimetry. Compensation, i.e. equal response[1] to the em and non-em shower components ($e/h = 1$), is only achieved in detectors with a small sampling fraction [1], whereas the best em performance is achieved with detectors that have a very large sampling fraction, or do not sample at all. However, the latter tend to deteriorate the hadronic performance of the calorimeter system of which they are part [2].

Our detector circumvents the problems associated with non-compensating calorimetry (poor hadronic resolution, signal non-linearity, non-Gaussian response function) by simultaneously measuring the energy deposit dE/dx (in the form of scintillation light) and the production of

*Corresponding author. Tel.: +1-806-742-3779; fax: (+1) 806 742-1182.
E-mail address: wigmans@ttu.edu (R. Wigmans).
[1]Following the convention introduced in Ref. [1], we define the *response* as the average calorimeter signal per unit of deposited energy.

0168-9002/$ - see front matter © 2004 Elsevier B.V. All rights reserved.
doi:10.1016/j.nima.2004.06.178

Cherenkov light in the shower development. The latter is almost exclusively generated by relativistic electrons and positrons in the electromagnetic shower component and, therefore, a comparison of the two signals makes it possible to determine the fraction of the shower energy deposited in em form (f_{em}) *event by event*. Since fluctuations in f_{em} are responsible for the poor performance of non-compensating calorimeter systems, and since these (dominant) fluctuations can be eliminated with this method, the performance of our detector is superior to what is commonly achieved with hadron calorimeters used in particle physics experiments [3]. Since this detector is not constrained to the small sampling fraction required for compensation, it is interesting to see what it can achieve in terms of electromagnetic shower detection.

This study is the topic of the present paper, which is organized as follows. In Sections 2 and 3, we describe the calorimeter and the experimental setup in which it was tested. In Section 4, we discuss the experimental data that were obtained and the methods used to analyze these data. Experimental results are described in Section 5. These include results on the response function, on the energy resolution, and on various contributions to this resolution, such as light yield, sampling fluctuations and sampling non-uniformities. We emphasize the differences between the two types of signals extracted from this calorimeter, which are very significant. Conclusions are presented in Section 6.

2. The DREAM detector

The measurements described in this paper were performed with a calorimeter that has become known by its acronym DREAM, for Dual-REAdout Module. The basic element of this detector (see Fig. 1) is an extruded copper rod, 2 m long and $4 \times 4\,mm^2$ in cross section. This rod is hollow, the central cylinder has a diameter of 2.5 mm. In this hole are inserted seven optical fibers. Three of these are plastic scintillating fibers[2], the other four

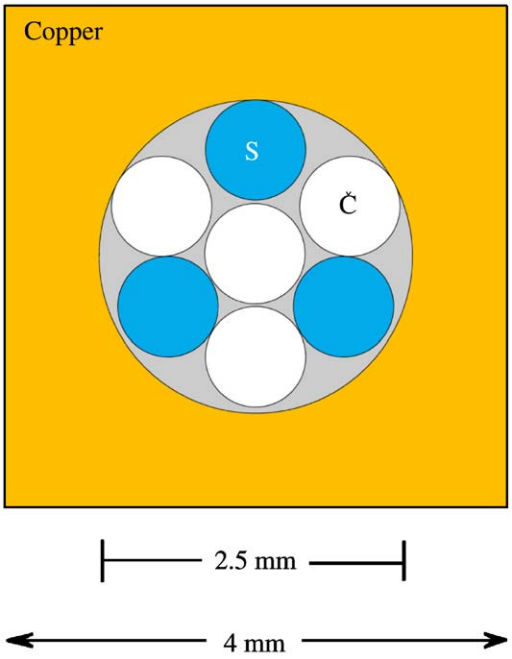

Fig. 1. The basic building block of the DREAM detector is a $4 \times 4\,mm^2$ extruded hollow copper rod of 2 m length, with a 2.5 mm diameter central hole. Seven optical fibers (four Cherenkov and three scintillating fibers) with a diameter of 0.8 mm each are inserted in this hole, as shown.

fibers are undoped. The latter are intended for detecting Cherenkov light and, therefore, we will refer to these in the following as *Cherenkov fibers*. We used two different types of Cherenkov fibers. For the central region of the detector, high-purity quartz fibers[3] were used, while the peripheral regions of the detector were equipped with acrylic plastic fibers[4]. The latter are a factor of 20 cheaper. All fibers had an outer diameter of 0.8 mm and a length of 2.50 m. The fiber pattern was the same for all rods, and is shown in Fig. 1.

The DREAM detector consisted of 5580 such rods, 5130 of these were equipped with fibers. The empty rods were used as fillers, on the periphery of the detector. The instrumented volume thus had a length of 2.0 m, an effective radius of $\sqrt{5130 \times 0.16/\pi} = 16.2\,cm$, and a mass of

[2]SCSF-81J, produced by Kuraray Co. Ltd, Tokyo, Japan.

[3]Polymer-clad fused silica fibers, produced by Polymicro, Phoenix, Arizona, USA.

[4]Raytela PJR-FB750, produced by Toray, Japan.

1030 kg. The effective radiation length (X_0) of the calorimeter was 20.1 mm, the Moliére radius (ρ_M) was 20.4 mm and the nuclear interaction length (λ_{int}) 200 mm. The composition of the instrumented part of the calorimeter was as follows: 69.3% of the detector volume consisted of copper absorber, while the scintillating and Cherenkov fibers occupied 9.4% and 12.6%, respectively. Air accounted for the remaining 8.7%. Given the specific energy loss of a minimum-ionizing particle (mip) in copper (12.6 MeV/cm) and polystyrene (2.00 MeV/cm), the sampling fraction of the copper/scintillating-fiber structure for mips was thus 2.1%.

The fibers were grouped to form 19 readout towers. Each tower consisted of 270 rods and had an approximately hexagonal shape (80 mm apex to apex). The effective radius of each tower was 37.1 mm ($1.82\rho_M$). A central tower was surrounded by 2 hexagonal rings, the Inner Ring (6 towers) and the Outer Ring (12 towers). The towers were not segmented in the longitudinal direction.

The depth of the copper structure was 200 cm, or $10.0\,\lambda_{int}$. The fibers leaving the rear of this structure were separated into bunches: one bunch of scintillating fibers and one bunch of Cherenkov fibers for each tower, 38 bunches in total. In this way, the readout structure was established (see Fig. 2). Each bunch was coupled through a 2 mm air gap to a photomultiplier tube (PMT).

We selected a 10-stage, 1.5″ PMT (Hamamatsu R-580) with a nominal gain of $3.7 \cdot 10^5$ at 1250 V. The larger gain needed for the readout of the Cherenkov fibers was obtained at approximately 1500 V, while the smaller gain needed for the readout of the scintillating fibers could not be reached by lowering the high voltage alone. Although the base with tapered voltage divider chosen (Hamamatsu E2183-501) was optimized for linearity, we did not want to lower the voltage so much that the linearity would be at risk. Thus we chose a high voltage of ~ 1000 V for the PMTs reading out the scintillating fibers and installed a yellow filter[5] between the fiber ends and the photocathode. To avoid a coupling capacitor in the anode signal path, we chose to have the anode near ground potential and the photocathode at negative high voltage. For best gain stability, we selected a PMT with an internal electrostatic shield surrounding the photocathode. This shield was held at the same potential as the photocathode. The PMT was surrounded by a high-permeability (10^5) μ-metal shield surrounded by a 5 mm thick iron shield. The μ-metal shield protruded more

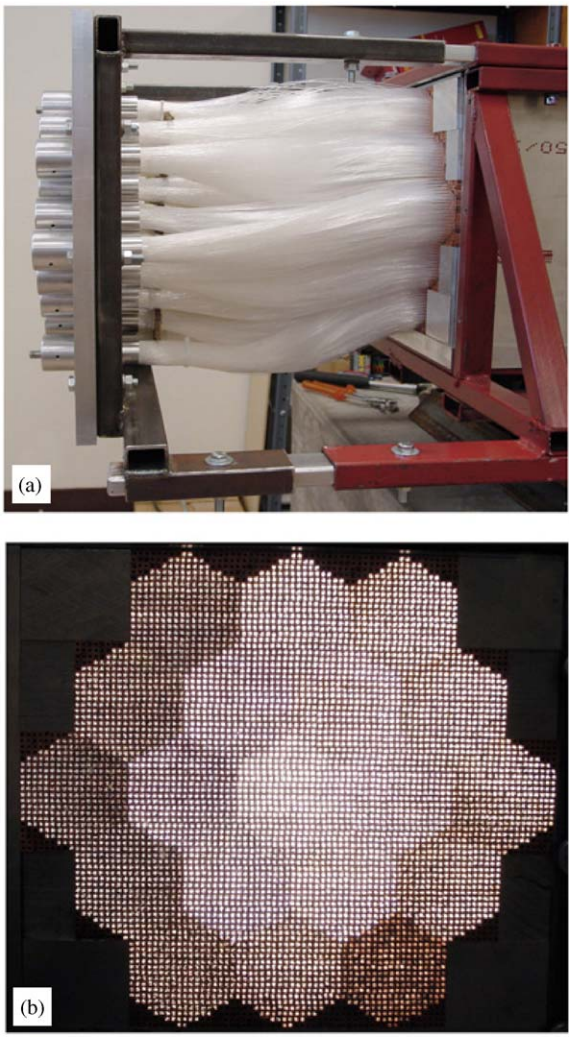

Fig. 2. The DREAM detector. Shown are the fiber bunches exiting from the downstream end of the detector (a), and an image of the front face while the fibers were illuminated with a bright lamp from the rear (b). The hexagonal readout structure is clearly visible.

[5]Kodak, Wratten #3, nominal transmission 7% at 425 nm, 90% at 550 nm.

than 1.5″ and the iron shield 2″ forward of the photocathode. This provided stability of the PMT gain when the beam tests required the calorimeter to be rotated and thus the direction of the Earth's magnetic field changed.

The yellow filter further had the advantage that it increased the attenuation length of the scintillating fibers substantially [4]. The blue part of the spectrum of light generated in the scintillating fibers is attenuated by self-absorption (resulting from overlap between the emission and absorption bands) and the yellow filter predominantly removed that part of the spectrum. The Cherenkov fibers did not suffer from significant longitudinal non-uniformity, their light attenuation characteristics were adequate without filtering (Section 5.2).

Fig. 2 shows photographs of the assembled detector. In Fig. 2a, the fiber bunches exiting the downstream end of the calorimeter and the 38 PMTs used to detect their signals are shown. In total, this detector contained about 90 km of optical fibers. Fig. 2b shows the front face of the calorimeter, when the fibers were illuminated with a bright lamp in the rear. The hexagonal readout structure is clearly visible.

3. Experimental setup

3.1. The beam line

The measurements described in this paper were performed in the H4 beam line of the Super Proton Synchrotron at CERN. The DREAM detector was mounted on a platform that could move vertically and sideways with respect to the beam. Changing the angle of incidence of the beam particles with respect to the fibers in the horizontal plane (the ϕ angle) and the vertical plane (the tilt angle, θ) was achieved with a crane. For the electron measurements described in this paper, we used four detector orientations:

(A) The "*untilted*" position, with ϕ and θ equal to 2° and 0.7°, respectively.
(B) The "*tilted*" position, with ϕ and θ equal to 3° and 2°, respectively.
(C) The "*z-scan*" position, with ϕ and θ equal to 24° and 0°, respectively. The orientation of the detector in this position is shown in Fig. 3.
(D) The "*untilted rotated*" position, with ϕ and θ equal to 6° and 0.7°, respectively.

The beam particle rates were typically several thousand per spill. The spills lasted 2.6 s and were repeated every 14.4 s. The widths of the collimators in the beam line were chosen so as to make the contribution of the momentum spread of the beam particles negligible. The purity of the electron beam varied considerably, depending on the energy and the collimator settings. In particular, high-energy electron beams were contaminated with pions and muons.

We used several auxiliary detectors in the beam tests. These detectors served to obtain nearly pure samples of incident particles and to measure the impact point of these particles in the calorimeter event by event. Fig. 4 shows a schematic overview of the beam line, in which the positions of these auxiliary counters are indicated:

- Two small scintillation counters provided the signals that were used to trigger the data acquisition system. These trigger counters (TC) were 2.5 mm thick, and the area of overlap was $6 \times 6\,\mathrm{cm}^2$. A coincidence between the logic signals from these counters provided the trigger.
- The impact point of the beam particles was measured with a *fiber hodoscope* (HOD). This

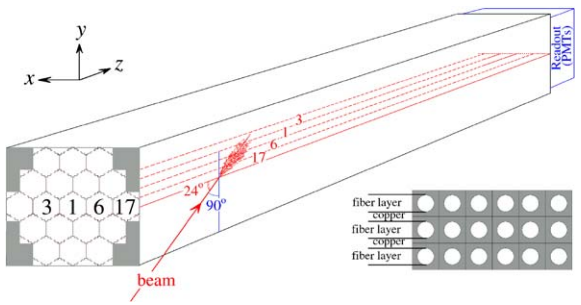

Fig. 3. Orientation of the DREAM calorimeter in the "*z-scan*" position, C(24°, 0°). The electron beams entered the detector in the horizontal ($x-z$) plane, at an angle $\phi = 24°$ with the direction of the fibers (the z-direction). The insert shows the fine-structure of the calorimeter, with horizontal fiber planes separated by layers of copper.

Fig. 4. Schematic view of the experimental setup in the beam line in which the DREAM detector was tested with electrons (see text for details).

hodoscope consisted of 2 ribbons of scintillating fibers oriented in the horizontal or vertical direction, thus providing the y and x coordinates of the beam particles. These hodoscope ribbons were originally developed in the context of the FAROS R&D project at CERN [5,6]. The fibers were 500 μm in diameter, the position resolution was ~ 200 μm and the probability that a charged particle generated a signal above threshold was ~ 95% for each ribbon. Each fiber ribbon was read out by a position sensitive photomultiplier tube[6]. Further details can be found in Refs. [5,6]. This hodoscope system was installed about 3 m upstream of the front face of the DREAM calorimeter. It made it possible to measure the coordinates of the impact point in the calorimeter with a precision of a fraction of 1 mm, depending on the beam energy. Several examples of the utility of this hodoscope are given in Section 5.

- The *preshower detector* (PSD) consisted of a 5 mm thick ($1X_0$) lead absorber, followed by a scintillation counter whose pulse height was recorded. This simple device turned out to be extremely useful to eliminate beam contamination and was an important tool in obtaining event samples of high purity.
- Downstream of the calorimeter, behind an additional $8\lambda_{\text{int}}$ worth of absorber, a $30 \times 30\,\text{cm}^2$ scintillation counter (MU) served to identify muons that contaminated the particle beam.

Especially at high energies (100 GeV and higher), the electron beam contained a substantial fraction of other particles, mainly pions and muons. Whereas the muons could be effectively identified and eliminated by using the fact that they can penetrate large amounts of material, the PSD was important for recognizing and eliminating the hadrons. Fig. 5 shows the signal distribution in the PSD for a 100 GeV electron beam. Most of the pions and muons contaminating this beam generated a signal consistent with a minimum-ionizing particle crossing the scintillator plane of the PSD, while almost all electrons generated a considerably larger signal. On their way through the $1X_0$ thick PSD absorber, electrons radiated a large number of photons. If one or more of these photons converted in the absorber, then the electrons and positrons generated in this conversion could add to the signal of the primary particle. When one photon converted

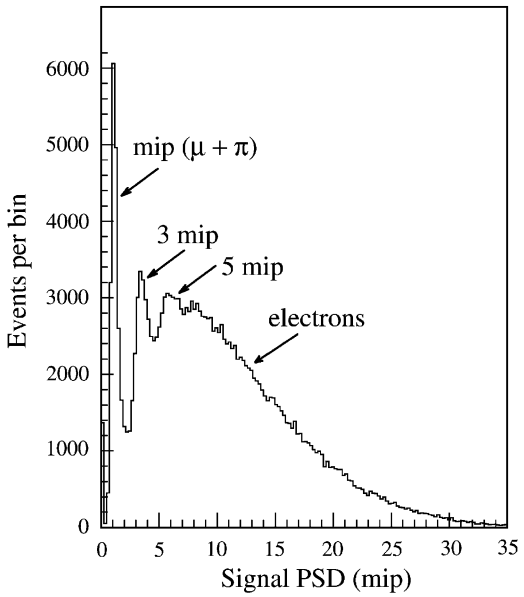

Fig. 5. Signal distribution for events recorded in the PSD for the 100 GeV electron beam. See text for details.

[6]Hamamatsu R2486, equipped with 16 × 16 anode wires for position detection.

into an e^+e^- pair inside the lead absorber and these particles traversed the scintillator plane, the result was thus a total signal equivalent to 3 times that of a mip. When two photons converted inside the absorber, the result was a signal equivalent to 5 times that of a mip, and so on. The distribution in Fig. 5 clearly exhibits peaks at 3 mip and 5 mip, as well as a continuum that stretches far beyond these peaks, up to 35 mip.

The PSD signal is thus an effective tool to distinguish between electrons and pions. By requiring a minimum value for this signal, most pions could be eliminated from the event samples, while most electrons passed the cut. An example of the results of such a procedure is given in Section 4.2.

3.2. Data acquisition

The various detector signals were transported through RG-58 cables with (for timing purposes) appropriate lengths to the counting room. There, the signals to be digitized (i.e. all except those from the trigger counters and the fiber hodoscope) were fed into charge ADCs. Two types of ADCs were used for these tests. Both types had a sensitivity of 4 counts/pC. The signals from the central tower and the inner ring were read out by 11-bit Lecroy 2249W ADCs, which have a range of 500 pC. The signals from the 12 towers constituting the Outer Ring (see Fig. 2b) were read out by 10-bit Lecroy 2249 ADCs, which have a range of 250 pC. The duration of the gate opened by the trigger signal was 120 ns, and the calorimeter signals arrived ~ 30 ns after the start of the gate.

The signals from the fiber hodoscope were fed into TDCs. In total, eight TDCs were used, four for the horizontal and four for the vertical fiber ribbons, respectively. The time information could be converted into (x, y) coordinates of the point where the beam particle traversed the hodoscope.

The data acquisition system was based on CAMAC, interfaced via a VME bus to a Linux-based computer. At maximum, 8000 events could be recorded per 2.6 s SPS spill. The typical event size was ~ 150 bytes. All calorimeter signals, as well as the signals from all auxiliary detectors, could be monitored on-line.

3.3. Calibration of the detectors

Using the high voltage, the gain in the PMTs was set to generate ~ 2 pC/GeV in the central detector tower, ~ 4 pC/GeV in the inner ring and ~ 6 pC/GeV in the outer ring of the DREAM calorimeter. By choosing different gains, we effectively extended the limited dynamic range of our readout and thus increased its sensitivity to small energy deposits in the shower tails.

Each of the 19 towers was calibrated with 40 GeV electrons. The photomultiplier gains were chosen in such a way that the average signal for 40 GeV electrons entering in the center of a tower corresponded to about 300, 600 or 900 ADC counts above the pedestal value in that tower, depending on the chosen gain. On average, $\sim 92\%$ of the scintillator light and $\sim 93\%$ of the Cherenkov light was generated in that tower. More precisely, the signals observed in the exposed tower corresponded to an energy deposit of 37.0 GeV in the case of the scintillating fibers and of 37.4 GeV for the Cherenkov fibers. This, together with the precisely measured values of the average signals from the exposed tower, formed the basis for determining the calibration constants, i.e. the relationship between the measured number of ADC counts and the corresponding energy deposit. The stability of the calibration was checked four times during the test period by sending 40 GeV electrons into the center of each calorimeter tower and measuring the signal distribution. The mean values of these distributions were reproduced to better than 2% in these measurements, for all channels and for the entire test period of 7 days.

4. Experimental data and methods

4.1. Experimental data

Events were triggered by coincident signals in the TC scintillation counters upstream of the calorimeter. Only events for which the (x, y) coordinates of the beam particle in the fiber hodoscope were measured were retained for the analyses described in this paper. One of purposes

of the hodoscope information was to be able to limit the impact region of the beam particles. For the analyses described in this paper, a circular region with a radius of 1.0 cm was selected.

The following data sets were used for these analyses:

(1) Electron data at 8, 10, 20, 40, 80, 100, 150 and 200 GeV, taken in the center of the DREAM calorimeter, with the detector oriented in the untilted position, A(2°, 0.7°).
(2) Electron data at the same eight energies, taken in the center of the calorimeter, with the detector oriented in the tilted position, B(3°, 2°).
(3) Electron data at the same eight energies, with the detector oriented in the z-scan position, C(24°, 0°). The impact point is indicated in Fig. 3.

Apart from these data sets, which were used for a systematic study of differences between the two readout media, we used the following data sets for some very specific purposes:

(4) Electron data at 8, 10, 20, 40, 80, 100, 150 and 200 GeV, taken with the detector oriented in position D(6°, 0°). These data were used for a study of the angular dependence of the Cherenkov shower signals (Section 5.7).
(5) Electron data at 40 GeV, taken with the beam steered into all individual towers, with the detector oriented in position A(2°, 0.7°). These data were used for an evaluation of the differences between the two different Cherenkov media (plastic and quartz) used in this detector (Section 5.6).
(6) A scan with 80 GeV electrons, performed in 15 steps of 1 cm in the central region of the calorimeter, with the detector oriented in position A(2°, 0.7°). These data were used to study signal non-uniformity and boundary effects between the calorimeter towers (Section 5.3).

4.2. Event selection

The procedures for obtaining clean electron samples are illustrated in Fig. 6, for the 150 GeV beam, which contained a substantial pion and muon contamination. Only $\sim 75\%$ of the recorded events were actually electrons.

Fig. 6a shows the PSD signal distribution, which is dominated by mips. The raw calorimeter signal distribution (the dashed curve in Fig. 6c) confirms the presence of contaminating muons and pions. After selecting events with a PSD signal in excess of 1.5 mip and no signal in the muon counter, there was no sign of any remaining muons, and a large fraction of the pions were removed as well (the solid curve in Fig. 6c). Note the logarithmic vertical scale in Fig. 6c. The small fraction of the remaining pions were events in which the PSD signal was larger than the cutoff value, either because the pion interacted in the PSD lead absorber or because it generated an event with a pulseheight in the Landau tail of the scintillator signals. This remaining contamination was removed by making use of the different lateral energy deposit characteristics. Electrons typically deposited more than 90% of their energy in the tower in which the shower developed, while the pion energy was distributed over several towers.

Fig. 6b shows the distribution of the fraction of the total scintillator signal recorded in the central tower, i.e. the tower into which the beam was steered. Studies of this variable for very pure electron event samples at lower energies showed that almost all electrons deposited at least 85% of their energy in this tower. By eliminating events for which this fraction was smaller than 0.85 from the 150 GeV event sample, the remaining hadrons were effectively removed. This is illustrated by the dotted curve in Fig. 6c, which shows the signal distribution for the almost pure electron event sample that remained after the cuts.

5. Experimental results

5.1. Electromagnetic response function

We start this section by presenting, in Fig. 7, the calorimeter signal distributions recorded for 40 GeV electrons with the detector in the untilted orientation (position A(2°, 0.7°), see Section 3.1). The signal distribution recorded with

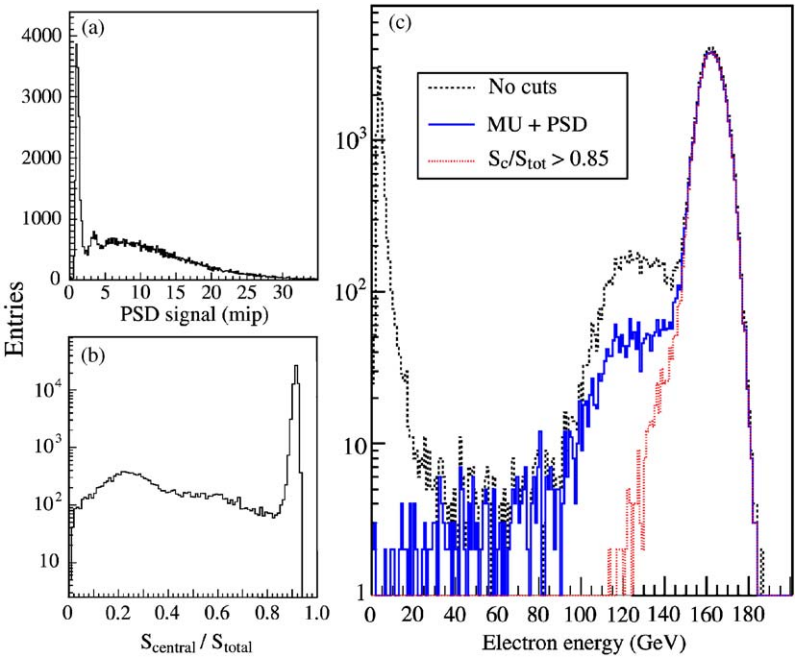

Fig. 6. The procedure for obtaining a pure 150 GeV electron sample. See text for details.

the scintillating fibers is shown in Fig. 7a, and the distribution of the signals from the Cherenkov fibers in Fig. 7b. A Gaussian fit describes the Cherenkov signals much better than the scintillator ones. The scintillator signal distribution exhibits a more or less flat plateau near its maximum. But upon closer inspection, also the Cherenkov distribution is not perfectly described by the fit, which has a reduced χ^2 of 4.5 (208 for 46 degrees of freedom). The χ^2/N_{dof} value of the fit to the scintillator distribution was 15 times worse.

The origin of these effects becomes clear when we look at similar distributions (for 100 GeV electron showers) with the detector oriented in the "*z-scan position*", C(24°, 0°) (see Fig. 3). The scintillator distribution exhibits a striking double-hump structure, that seems as if it is the result of a superposition of two distributions with different mean values (Fig. 8a). The variable distinguishing these separate distributions is the *y*-coordinate of the impact point of the electron. This coordinate was determined with

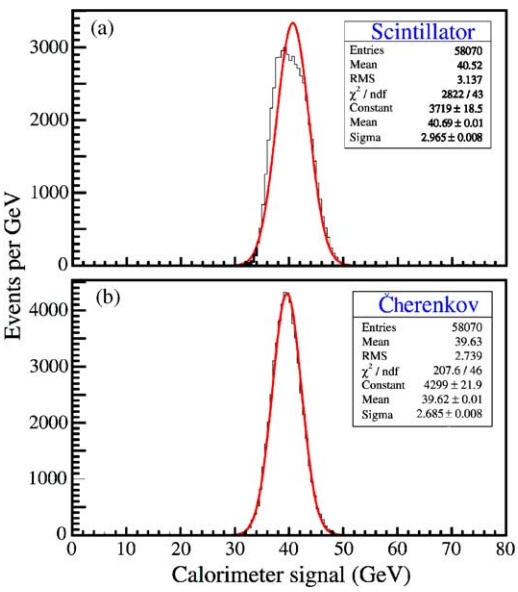

Fig. 7. Signal distributions for 40 GeV electrons, recorded from the scintillating (a) and the Cherenkov (b) fibers, with the DREAM calorimeter in the untilted position, A(2°, 0.7°).

the horizontal fiber hodoscope. Fig. 8b shows the signal distribution for a sample of events where the particles entered the detector in a horizontal fiber plane. The distribution in Fig. 8c is for a sample of events in which the entry point was located in the 1.5 mm thick copper plane that separates these horizontal fiber layers (see Figs. 1 and 3). Clearly, the sampling fraction, and thus the resulting calorimeter response, is different for these two event samples. The response is smaller for particles entering the detector in the copper.

This can be concluded from the results shown in Fig. 9, where this phenomenon is analyzed in more detail. Fig. 9a shows the total scintillator signal as a function of the y-coordinate of the impact point. The impact region (a circle with a radius of 10 mm) was subdivided into y-bins of 0.5 mm width, using the hodoscope information. Figs. 9b, c and d depict the contributions of Towers 17, 6 and 1 to the total scintillator signal, also as a function of the y-coordinate of the impact point. As can be seen in Fig. 3, these are the towers sequentially traversed by the showering particle, and more than 95% of the total shower energy was deposited in these three towers.

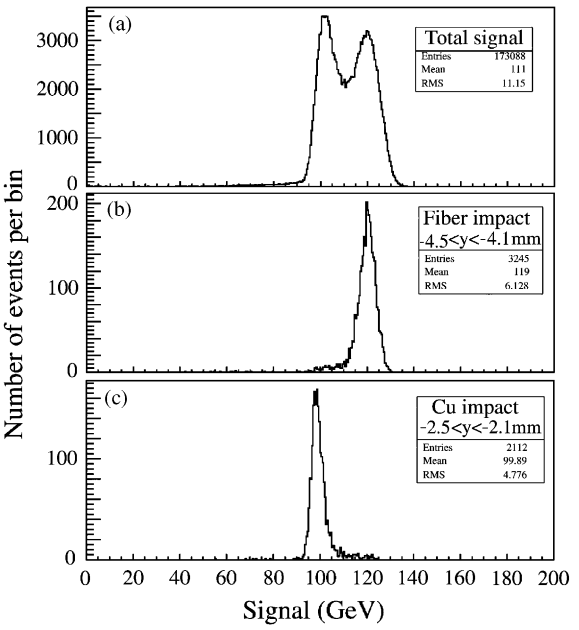

Fig. 8. Signal distributions for 100 GeV electrons, with the DREAM calorimeter in the z-scan position, C(24°, 0°). Shown are the total scintillator signal distributions regardless of the impact point (a) and for electrons entering the detector in a horizontal fiber layer (b), or in the copper in between such layers (c).

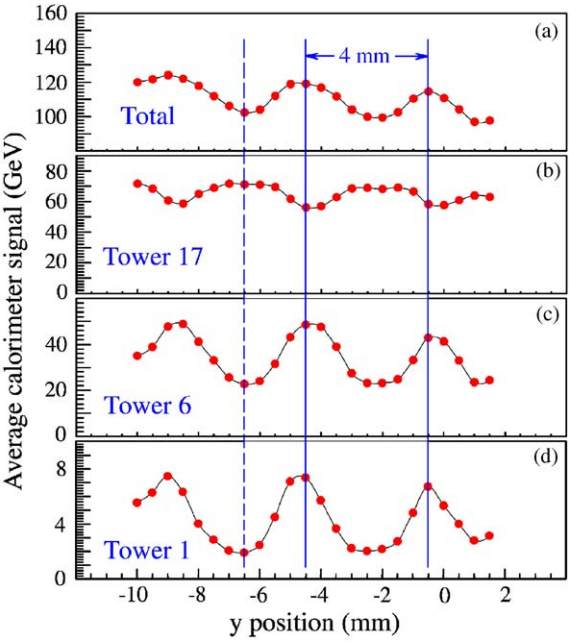

Fig. 9. Average scintillator signal as a function of the y-coordinate of the impact point, for 100 GeV electrons entering the DREAM calorimeter in the z-scan position, C(24°, 0°). Shown are the averages for the total signal (a), and for the signals recorded in towers 17 (b), 6 (c) and 1 (d). The solid vertical lines represent the locations of horizontal fiber planes, the dashed line indicates the center of a copper plane that separates such fiber planes. See Fig. 3 for geometric details.

The total signal exhibits an oscillating pattern with a characteristic distance scale of 4 mm, i.e. exactly the transverse dimension of the tubes of which the DREAM calorimeter is composed (see Fig. 1). A comparison of the different distributions in Fig. 9 reveals that maxima in the total response correspond to maxima in the signals recorded in Towers 6 and 1, and *minima* in the signals from Tower 17. At an angle of 24°, the effective thickness of the DREAM towers is 17.7 cm, i.e. the shower develops in a number of longitudinal segments with a depth of $8.8X_0$ each. However, in the early stages of its development (before reaching the shower maximum), the shower is very

narrow. That is, narrow in comparison with the 4 mm pitch of the DREAM structure. Therefore, the effective thickness of the *first* longitudinal segment, Tower 17, depends on the impact point of the particles. If the electron enters in the copper, this effective depth is closer to that of a pure copper absorber ($\sim 12X_0$), while the effective depth is much less for showers developing in the "Swiss-cheese" portion of the structure, i.e. in the horizontal fiber planes ($\sim 6X_0$).

Particles entering the calorimeter in these fiber planes therefore deposit a much smaller fraction of their total energy in Tower 17 than do particles entering in the copper. In the latter case, the shower maximum is located inside Tower 17 and the deeper segments (Towers 6 and 1) only sample the tails of the showers. Particles entering in the fiber planes deposit a much smaller fraction of their total energy in Tower 17, thus yielding a smaller signal in this tower than the electrons entering in the copper. On the other hand, the energy fraction and thus the resulting signals are much larger in the deeper segments, Towers 6 and 1. And because the early, highly collimated portion of the shower is more efficiently sampled for the particles entering in the fiber planes, the *total* scintillator response is also larger in this case. The data shown in Fig. 9 thus make it clear that the larger of the two response values observed in Fig. 8 corresponds to particles entering the detector in the horizontal fiber planes.

The size of the effects in Fig. 9 illustrates that a considerable fraction of the shower energy is deposited within a few mm from the shower axis, i.e. on a distance scale comparable to the pitch of the absorber structure (4 mm). Therefore, the precise location of that shower axis is crucially important. In the *z-scan* measurements, the axis can be *entirely* located in copper, since $\theta = 0$ in this geometry. In that case, the energy deposited within 0.75 mm from the shower axis may not be sampled at all.

The effects of this sampling inefficiency, and the resulting sampling non-uniformity, depend very sensitively on the angles ϕ and θ between the shower axis and the fiber direction. This becomes clear from Fig. 10, which shows the average scintillator signals for 100 GeV electrons measured with the calorimeter oriented in the *untilted* position, A(2°, 0.7°). In Fig. 10a, the average signal is given as a function of the y-coordinate of the impact point. As before, the impact region was subdivided into 0.5 mm wide y-bins for this purpose. Fig. 10b depicts the x-dependence of the signals. The characteristic oscillations are present in both cases, however they are much less pronounced in the x-case, where the shower axis makes a 2° angle with the (vertical) fiber planes. The particles near the shower axis are thus sampled every $1.5/\sin 2^\circ = 43$ mm, or $\sim 2X_0$. On the other hand, the shower axis makes an angle of only 0.7° with the horizontal plane. Therefore, when electrons enter the calorimeter in a horizontal copper layer, the shower particles near the axis are only sampled every $1.5/\sin 0.7^\circ = 123$ mm, or $\sim 6X_0$. As a result, the sampling non-uniformities are much more pronounced when event samples are selected according to their y-coordinates than to their x-coordinates.

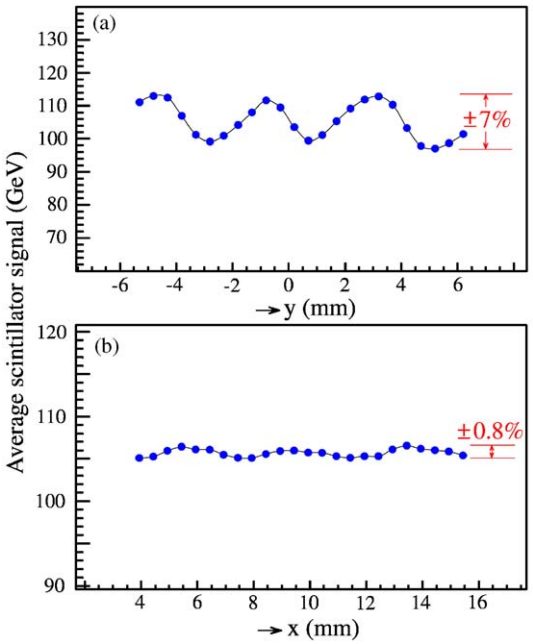

Fig. 10. Average scintillator signal as a function of the y-coordinate (a) and of the x-coordinate (b) of the impact point, for 100 GeV electrons entering the DREAM calorimeter oriented in the untilted position, A(2°, 0.7°). Note the different vertical scales.

So far, we have only looked at the scintillator signals. However, it is interesting to compare the described effects with those observed for the Cherenkov signals. Fig. 11b shows how the average Cherenkov signal varies with the y-coordinate of the impact point. The same oscillations that were observed for the scintillator signals (Fig. 11a) are also present in this case, but they are clearly less pronounced. Fig. 11b also exhibits some indication of a gradual overall change of the Cherenkov response over the impact region. This is consistent with the results of detailed studies of non-uniformities in the central calorimeter region (see Fig. 18b).

In Fig. 12, the energy dependence of these effects is shown separately for both detector orientations, A(2°, 0.7°) and B(3°, 2°). The fractional difference between the maximum and minimum values of the calorimeter response is given as a function of energy, for both the scintillator and the Cherenkov signals. In both detector orientations, the effects are considerably smaller for the latter. A comparison of both panels

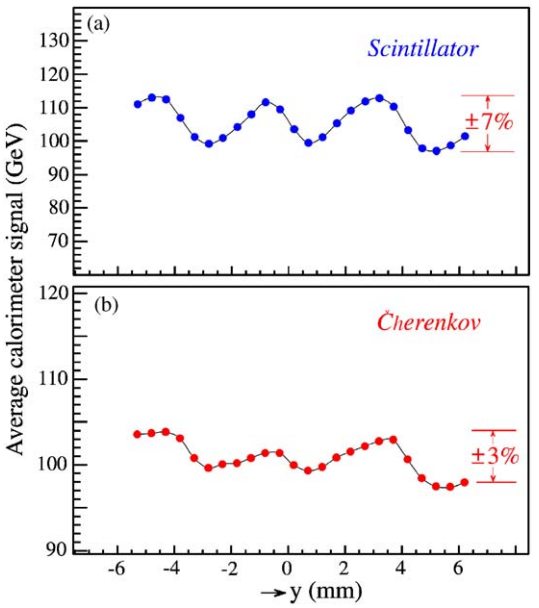

Fig. 11. Average calorimeter signal as a function of the y-coordinate of the impact point, for the scintillator (a) and Cherenkov (b) signals from 100 GeV electrons entering the DREAM calorimeter oriented in the untilted position, A(2°, 0.7°). Note the different vertical scales.

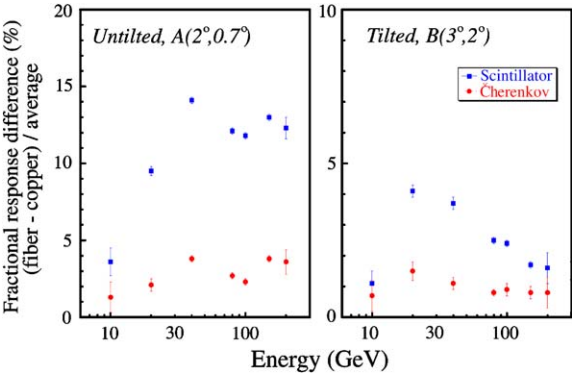

Fig. 12. The average fractional difference between the response for particles entering the DREAM calorimeter in a horizontal fiber layer and the response for particles entering in the copper in between such layers. Results are given separately for the scintillator and Cherenkov signals, with the detector oriented in the untilted position, A(2°, 0.7°) (left) or the tilted position, B(3°, 2°) (right).

also shows the dramatic decrease in the effects for the scintillator signals that results from a small increase in the tilt angle. At low energies, the differences between the average signals from particles entering the detector in a horizontal fiber plane and in the copper in between such planes seems to decrease. This is not a real effect, but rather reflects the fact that at low energies the correlation between the hodoscope coordinates and the impact point of the particle in the calorimeter deteriorates, mainly as a result of increased beam dispersion and multiple scattering in the material in between the hodoscope and the calorimeter.

In evaluating the consequences of the results depicted in Figs. 10–12 for the calorimeter performance, one should realize that the systematic uncertainty in the calorimeter response for a particle entering the detector at a random position is represented by the σ_{rms} value of distributions such as those shown in Figs. 10 and 11. The results from Fig. 12 concern the relative difference between the maximum and minimum values of such distributions, which for sinusoidal distributions corresponds to $2\sqrt{2}\sigma_{\mathrm{rms}}$.

The differences observed in Fig. 12 between the scintillator and Cherenkov signals allow for an

interesting conclusion. Apparently, the particles that contribute to the Cherenkov signals have a lateral shower profile that is not as strongly concentrated near the shower axis as in the case of the scintillator signals. This may be understood from the fact that the particles that generate a signal in the Cherenkov fibers need to traverse these fibers at an angle that is not very different[7] from the Cherenkov angle ($\theta_C \approx 46^\circ$) [7]. Such particles are predominantly produced in the later stages of the shower development, mainly through Compton scattering [1]. The shower particles produced in the early stages of the em shower development originate mainly from $\gamma \to e^+e^-$ conversions and travel almost parallel to the direction of the showering particle. Therefore, the particles responsible for the early, narrow portion of the energy deposit profile *do* contribute to the scintillator signals, but *not* to the Cherenkov signals. Explicit measurements of the shower profiles, as well as detailed Monte Carlo simulations, which are described in Ref. [8], confirmed this conclusion.

Since a substantial fraction of the em shower energy is deposited within a few mm of the shower axis, the sampling fraction (and thus the calorimeter response) may become (strongly) dependent on the location of the impact point of the particles. However, if this impact point is fixed, then the signal distributions become narrow and Gaussian, as illustrated in Fig. 8. This effect is also apparent from Fig. 13, which shows the quality of Gaussian fits to the signal distributions, for measurements carried out with the detector oriented in position B(3°, 2°). The χ^2/N_{dof} values of such fits gradually increase with energy, which can be understood from the fact that a superposition of two Gaussian distributions with different mean values looks less like one Gaussian when the widths of the two individual distributions decrease (i.e. as the energy increases). However, when event samples were selected with the same impact point, the Gaussian fits became almost perfect, with χ^2/N_{dof} values around 1, for the entire energy range, both for the scintillator and the Cherenkov signal distributions.

[7]The trapping cone has an opening angle of 19° for the quartz fibers and 30° for the plastic ones.

In summary, all effects described in this subsection are due to non-uniformities in the sampling fraction, which translate into a non-uniform calorimeter response. The magnitude of the effects is extremely sensitive to the angle of incidence of the particles. They are very substantial when the particles enter the detector in a plane that is parallel to the fiber planes (Fig. 8). However, when the angles between the shower axis and the horizontal and vertical fiber planes *both* are larger than $\sim 2^\circ$, the effects become negligibly small (Figs. 10b, 12). All effects are much smaller for the Cherenkov signals than for the scintillator signals, as a result of the different lateral shower profiles.

In the following subsections, we will encounter several other experimental consequences of these characteristics.

5.2. Linearity

Signal linearity is best studied through the calorimeter response, i.e. the average signal per unit of deposited energy. In a linear calorimeter,

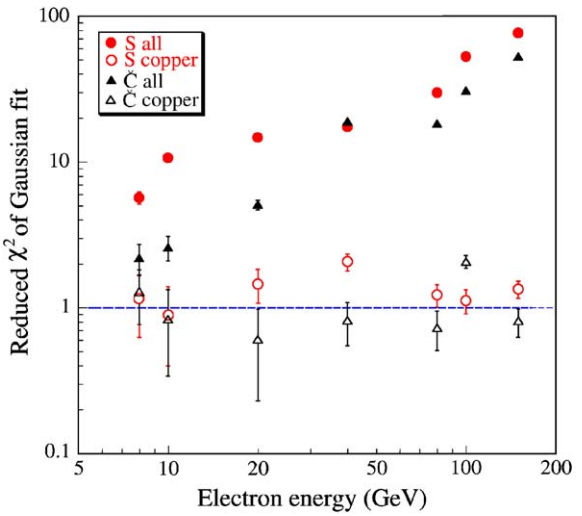

Fig. 13. The quality of a Gaussian fit (expressed in terms of the reduced χ^2 of that fit) is shown as a function of energy for both the scintillator and the Cherenkov signal distributions. Also shown are the χ^2/N_{dof} values for event samples in which the electrons entered the calorimeter at a fixed point, in the copper between horizontal fiber layers.

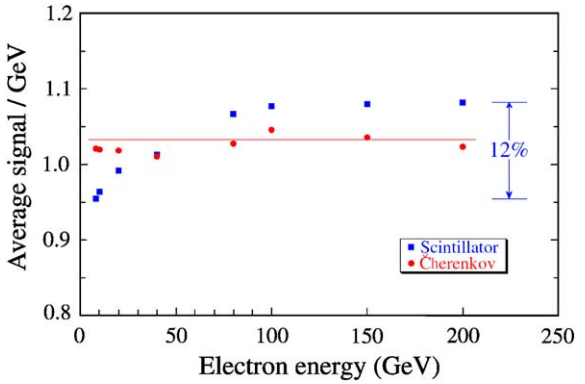

Fig. 14. The response for electrons entering the DREAM calorimeter oriented in the tilted position, B(3°, 2°), as a function of energy. Results for the scintillating fibers (squares) and the Cherenkov fibers (circles) are shown separately. Note the zero-suppressed vertical scale. The data are normalized to the response for 40 GeV electrons, obtained in the calibration runs. This response was ~ 1% smaller than that in the energy scans. The statistical errors are smaller than the size of the symbols. Systematic errors, dominated by gain instabilities, are at the 1–2% level.

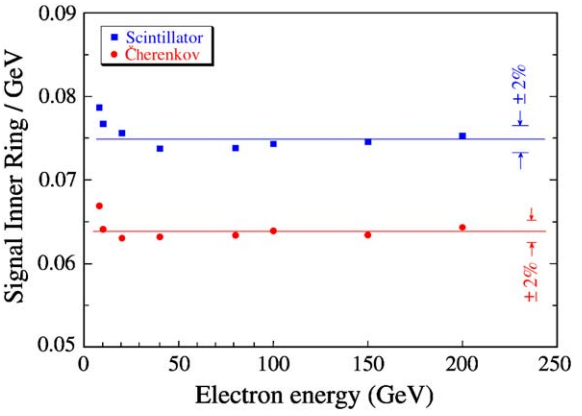

Fig. 15. The response for small energy deposits in the tails of em showers, as a function of the shower energy. Results are shown separately for the signals from the scintillating (squares) and the Cherenkov fibers (circles). See text for details.

the *response is constant*, independent of the deposited energy.

Fig. 14 shows the response of the DREAM calorimeter to electrons in the energy range 8–200 GeV, for the scintillator and the Cherenkov signals. The detector was oriented in the tilted position, B(3°, 2°), when these data were taken, but the results in the untilted position, A(2°, 0.7°), are very similar.

The Cherenkov response is seen to be nearly constant. Deviations from linearity are smaller than 2% over the entire energy range. On the other hand, the scintillator signals exhibit a large non-linearity: The response at 8 GeV is ~ 12% smaller than that at 200 GeV.

To investigate the cause(s) of this effect, we first studied the signals in the inner ring surrounding the central tower into which the electron beams were steered. Since the lateral em shower profiles scale with energy [1], the percentage of the shower energy deposited in this inner ring should be constant. We found it to be ~ 7.5% for the scintillator signals and ~ 6.5% for the Cherenkov signals[8]. Fig. 15 shows that the scintillator signals were very linear for the small energy deposits in the tails of the showers. The non-linearity must thus originate in the central tower, where more than 90% of the shower energy was deposited.

The direction of the non-linearity is somewhat unusual. Typically, non-linearity in light-based calorimeters manifests itself at the high-energy end of the spectrum, as a result of saturation effects in the light detectors or shower leakage. We investigated three possible effects that might cause non-linearity at low energies in the scintillator signals and, important, would *barely* affect the Cherenkov signals:

(1) *Light attenuation* in the fibers. We measured the light attenuation characteristics of the fibers with the detector in the *z-scan* position, C(24°, 0°), as depicted in Fig. 3. A beam of 40 GeV electrons was used for this purpose. By moving the impact point of the particles in steps of 1 cm, the effective depth z of the light production in the fibers was changed in steps of $1/\sin 24^\circ \approx 2.5$ cm.The average signals are shown as a function of z in Fig. 16. The signals are normalized to the one measured in the most upstream position. The curves through the data points have been drawn to guide the eye. They show that the scintillator signals increase, on average, by 0.2% per cm in the

[8]This difference is very interesting in its own right. It is discussed in detail in [8].

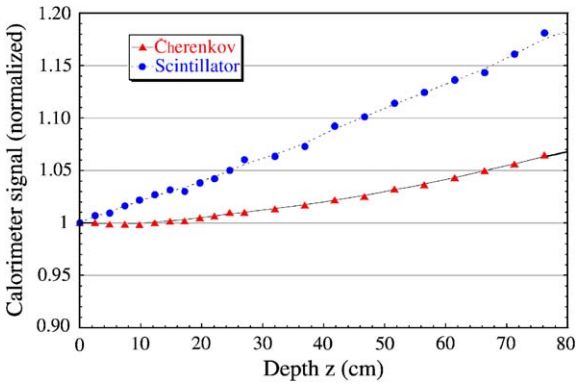

Fig. 16. The effects of light attenuation in the scintillating and the Cherenkov fibers. The average signals from 40 GeV electron showers are shown as a function of the (effective) depth at which the light production takes place. The curves are drawn to guide the eye. See text for details.

first 20 X_0, i.e. the region displayed in the figure. This increase corresponds to an attenuation length of ~ 5 m. The increase in the Cherenkov signals was a factor of 3 smaller, averaged over this region. In the upstream portion of the detector (low z values), where the development of em showers takes place, the difference was even considerably larger: over a distance of 30 cm ($15X_0$), the Cherenkov signal changed only by $\sim 1\%$.

The light attenuation in the scintillating fibers was thus much stronger than in the Cherenkov fibers. This difference is a result of self-absorption caused by the overlapping absorption and emission spectra of the wavelength shifting dopants in the scintillating fibers, an effect that was greatly reduced by eliminating the blue light component by means of yellow filters. The light production in high-energy showers takes place, on average, deeper inside the detector than in low-energy showers. The light from the low-energy showers is thus more attenuated and the resulting response is smaller. Therefore, light attenuation in the scintillating fibers does indeed lead to a non-linearity with the observed characteristics. Because of the virtual absence of light attenuation in the region where em showers develop, this type of non-linearity is completely negligible for the Cherenkov signals.

(2) *Energy loss* in upstream material. This upstream material does not only include the Preshower Detector ($1X_0$ of lead) and a 2 mm thick aluminium front cover plate, but also the first radiation length of the copper absorber. This is because the fibers in the central calorimeter tower started about 1 cm deep inside the absorber structure. The energy fraction deposited in this "dead material" depends upon the shower energy. The lower the electron energy, the larger this fraction becomes. Therefore, this effect also causes a signal non-linearity of the observed type. The reason why this effect is inconsequential for the Cherenkov signals is the fact that energy deposited in the first few radiation lengths barely contributes to the Cherenkov signals. In this very early stage of the shower development, the profile is extremely narrow and the energy is almost exclusively deposited by fast electrons and positrons from converting γs radiated by the incoming particle. Such electrons do of course contribute to the scintillator signals, but *not* to the Cherenkov signals, which are constituted by shower particles traversing the fibers at or near the Cherenkov angle. Such particles are abundantly produced at greater depth, but are virtually absent in the first few radiation lengths.

(3) *Sampling inefficiencies*. The very small angles between the shower axes and the fibers have consequences, not only for the response uniformity and the em energy resolution of this calorimeter, but also for the efficiency with which the early, highly collimated shower component is sampled. No matter where the particles enter the detector, there is always a cylindrical volume with a radius of ~ 1 mm and a length of ~ 4 cm where the early shower finds only copper on its way. The fraction of the shower energy deposited in this "dead" copper cylinder depends on the energy of the incoming electron: the lower the energy, the larger the fraction. For example, in a 10 GeV shower, 8.6% of the total energy is deposited in a cylinder with a radius of 1 mm, stretching from $2X_0$ (the end of the dead material upstream) to $5X_0$ (4 cm deeper). A200 GeV

shower deposits only 3.1% of its energy in the same region. This difference corresponds to about half of the measured signal non-linearity. Again, the Cherenkov signals are practically immune to this effect, since their lateral shower profiles in this early stage of the shower development are not as steep as for the scintillator signals.

We determined the magnitude of the three mentioned effects by means of EGS4 Monte Carlo simulations, the results of which are shown in Fig. 17. It turned out that effects 2 and 3 dominate and that the three effects combined reproduce the observed non-linearity fairly well.

There are several conclusions to be drawn from this. First, a detector based on optical fibers running in approximately the same direction as the incoming particles is more uniform and linear when the signals are based on the Cherenkov effect than on a measurement of energy deposit. In the previous subsection, we saw that this conclusion applied to the impact point dependence of the signals. In Section 5.4, we will see that it applies to the energy resolution. And as we see here, it also applies to the em signal linearity. The second conclusion is that none of the effects causing the observed non-linearity in the scintillating fibers is of any consequence for the detection of hadrons and jets, the main purpose of this detector and the basis for its design. Energy losses in upstream material are much smaller, and the lateral energy deposit profiles are much broader for hadronic showers than for em ones. The effects of light attenuation can be corrected event-by-event [3]. A calorimeter of this type could also be constructed in such a way that all the mentioned effects contributing to the non-linearity for em showers are essentially avoided or correctable.

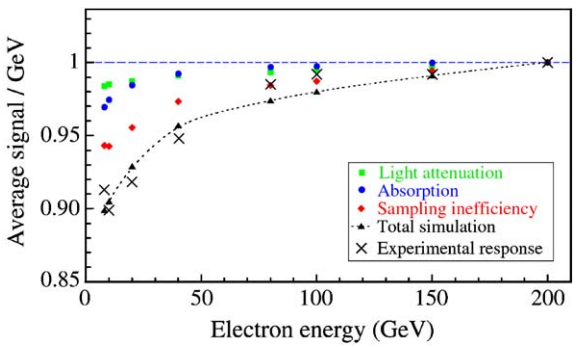

Fig. 17. Analysis of the origin of the non-linearity of the scintillating-fiber signals. The crosses represent the experimental response, as a function of the electron energy, with the detector oriented in the untilted position, A(2°, 0.7°). The squares indicate the effect of light attenuation in the fibers alone, the circles the effect of energy absorption in upstream material, and the diamonds the effect of the energy-dependent sampling inefficiency. The triangles represent the cumulative effects of all three sources of non-linearity combined. See text for details.

5.3. Signal uniformity

Whereas the signal uniformity studied in Section 5.1 concerns variations on the scale of a few mm, i.e. the size of one copper tube, the uniformity addressed in this subsection concerns variations over the entire surface of an (hexagonal) readout tower (i.e. 270 copper tubes), and in particular near the boundaries between towers. Non-uniformities observed on this scale may be caused by variations in fiber quality (light yield, attenuation) and/or in the quantum efficiency of the PMT's photocathode.

The signal uniformity was studied using data from a position scan, in which a 80 GeV electron beam was moved in steps of 1 cm across the central region of the calorimeter (dataset 6, see Section 4.2). The calorimeter signal, averaged over 4 mm wide bins in the x-coordinate, is shown in Fig. 18 as a function of x. The figure also shows the contributions of three individual towers to the signals measured at the various positions. The detector turned out to be quite uniform, especially for what concerned the scintillator signals (Fig. 18a). Deviations from the average response were small, $\sim 1.8\%$ (σ_{rms}). In particular, the boundaries between the different hexagonal cells are barely noticeable.

The uniformity was not as good for the Cherenkov signals. Here, deviations from the average response had an rms value of 3.2%. Since the fluctuations responsible for these deviations are independent of the shower energy, they may be expected to contribute an energy-independent term to the em energy resolution.

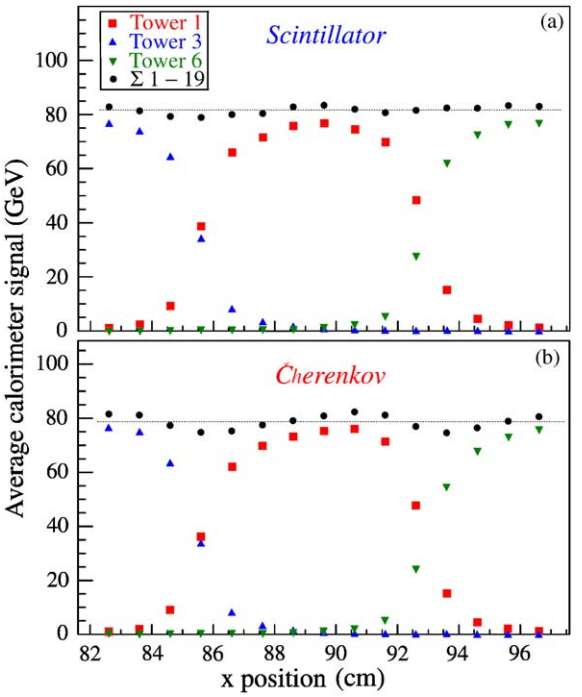

Fig. 18. The response to 80 GeV electrons as a function of their impact point. Each point represents a bin with a width of 4 mm, the width of the copper tubes. Results are shown for the signals from the scintillating (a) and the Cherenkov (b) fibers. Error bars are smaller than the data points in all cases.

5.4. Electromagnetic energy resolution

The non-uniformities described in the previous subsections have also important repercussions for the electromagnetic energy resolution of the DREAM calorimeter, σ/E. Unless stated otherwise, resolutions mentioned in the following were determined from Gaussian fits to the signal distributions, covering a region of $\pm 4\sigma_{\mathrm{rms}}$ around the mean value.

In a sampling calorimeter, the em energy resolution is usually dominated by sampling fluctuations and (in the case of Cherenkov readout) photoelectron statistics, both of which are governed by Poisson statistics and thus lead to the familiar $E^{-1/2}$ term. However, response non-uniformities such as those described in the previous subsections lead to a deviation from $E^{-1/2}$ scaling, the effects of which become dominant at high energies.

This is illustrated in Fig. 19, which shows the energy dependence of the em energy resolution, for two different detector orientations: The *tilted* and *untilted* orientation. The numerical values of the measured resolutions are also listed in Table 1. The relevant difference between the two detector orientations is the tilt angle θ, which is 2° and 0.7°, respectively. This difference had substantial consequences for the em energy resolution. In Fig. 19a, the abscissa is $E^{-1/2}$, which has the advantage that $E^{-1/2}$ scaling is represented by a straight line in this plot. The experimental data were fit with the formula

$$\frac{\sigma}{E} = \frac{a}{\sqrt{E}} + b \tag{1}$$

which provided a reasonable description of these data. However, both the values of a and b were very different for the two data sets, which only differed in the tilt angle θ. This is a strong indication that this description is fundamentally incorrect, since the factors determining the value of a (sampling fluctuations, photoelectron statistics) should not change when the tilt angle of the detector is changed by only 1.3°.

In Fig. 19b, the *same* experimental data are plotted in a different way. Here, the abscissa is E^{-1}, while the ordinate is $(\sigma/E)^2$. In this representation, a straight line describes a relationship of the type

$$\frac{\sigma}{E} = \frac{A}{\sqrt{E}} \oplus B. \tag{2}$$

Linear fits to these experimental data now yielded the same value for A ($\sim 24\%$), but differed in the value of B: 6.7% for $\theta = 0.7^\circ$, 2.8% for $\theta = 2^\circ$. In this description, the effect of the response uniformity is thus treated as an energy-independent, i.e. constant, term added in quadrature to the $E^{-1/2}$ scaling term. The latter is independent of the tilt angle, as it should.

However, as indicated by the χ^2 values (see Table 2), also this description is not entirely accurate, especially for the scintillation channel. The 20 and 40 GeV points are lying more than four standard deviations above the fitted curve,

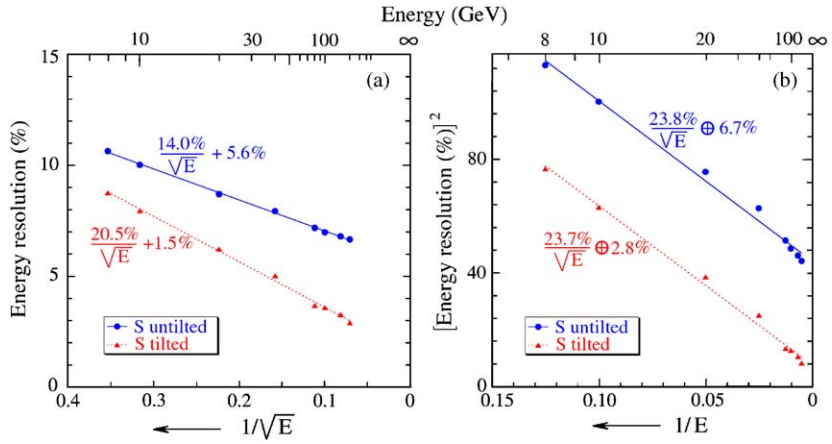

Fig. 19. The energy resolution as a function of energy, for electron signals recorded in the scintillating fibers. Results are shown for two detector orientations, which differ only in the tilt angle of the calorimeter, $\theta = 0.7^\circ$ (circles) and 2° (triangles), respectively. In panel *a*, the resolution is plotted as a function of $1/\sqrt{E}$. In panel *b*, the same experimental results are displayed in a different way, here the square of the energy resolution is plotted as a function of $1/E$.

Table 1
The electromagnetic energy resolutions measured in the scintillation and Cherenkov channels, with the DREAM detector oriented in the untilted position, A(2°, 0.7°), and in the tilted position, B(3°, 2°)

Energy	*Untilted*, A(2°, 0.7°)		*Tilted*, B(3°, 2°)	
(GeV)	S	C	S	C
8	10.64±0.18	14.15±0.25	8.76±0.07	13.51±0.10
10	10.02±0.10	13.14±0.13	7.95±0.06	12.12±0.10
20	8.70±0.04	9.08±0.05	6.22±0.03	8.88±0.03
40	7.93±0.03	6.66±0.03	5.02±0.02	6.52±0.02
80	7.18±0.03	4.98±0.02	3.68±0.01	4.89±0.02
100	6.98±0.03	4.63±0.03	3.58±0.01	4.52±0.02
150	6.80±0.03	4.00±0.03	3.27±0.02	4.10±0.02
200	6.66±0.12	3.47±0.06	2.90±0.04	3.63±0.05

The resolution was determined from a Gaussian fit to the signal distribution, covering a region of $\pm 4\sigma_{\mathrm{rms}}$ around the mean value. For the scintillator signals in the untilted position, whose distributions exhibited large deviations from a Gaussian line shape, the resolution was determined on the basis of σ_{rms}. All resolutions are given in %, the errors are statistical only.

whereas the high-energy points are systematically located (up to 10 σ) below this curve. The values of B thus tend to systematically underestimate the resolutions at the highest energies. For example, the energy resolution measured at 200 GeV in the tilted position was $2.90 \pm 0.04\%$, whereas the fit with (2) predicts 3.26%. This might be an indication that the description of the effect of non-uniformity of the response on the em energy resolution by means of a constant term is an oversimplification and in fact depends on the energy of the showering particle. As we saw in Section 5.1, the non-uniformities arise from sampling inefficiencies in the early, highly collimated part of the shower. As the energy increases, the shower penetrates deeper inside the calorimeter structure and this early component represents a decreasing fraction of the total shower energy. Therefore, it would be no surprise to find that the deviation from $E^{-1/2}$ scaling of the em energy

Table 2
Results of the fits of expressions of the types $\sigma/E = aE^{-1/2} + b$ and $\sigma/E = AE^{-1/2} \oplus B$ to the measured experimental energy resolutions

Coefficient	*Untilted*, A(2°, 0.7°)		*Tilted*, B(3°, 2°)	
	S	C	S	C
a	14.0 ± 0.2	38.2 ± 0.4	20.5 ± 0.3	34.9 ± 0.4
b	5.6 ± 0.1	0.8 ± 0.1	1.5 ± 0.2	1.1 ± 0.2
χ^2/N_{dof}	22/6	94/6	373/6	125/6
A	23.8 ± 0.3	40.0 ± 0.6	23.7 ± 0.3	37.5 ± 0.5
B	6.7 ± 0.2	2.2 ± 0.3	2.8 ± 0.2	2.6 ± 0.2
χ^2/N_{dof}	137/6	26/6	910/6	47/6

All numbers are given in %. The χ^2 values were calculated on the basis of statistical errors only.

resolution decreases as well. The value of B found in fits of the experimental data to Eq. 2 would then be an average value, too high at high energies and too low at low energies. Table 2 summarizes the results of the fits of expressions (1) and (2) to the measured energy resolutions.

A comparison of the fit results in Figs. 19a and b shows that the difference between the values of the scaling parameter (a, A) found with expressions (1) and (2) rapidly grows with the value of the constant term (b, B). For small deviations from $E^{-1/2}$ scaling, both expressions become equivalent. Such small deviations occur in Fig. 20, where the em energy resolutions for the two readout media of our calorimeter are compared, for the tilted orientation, B(3°, 2°). This comparison shows that the $E^{-1/2}$ term for the quartz readout is larger than that for the scintillating fibers. On the other hand, the deviation from $E^{-1/2}$ scaling is somewhat smaller for the signals measured with the Cherenkov fibers (see also Table 2).

For small tilt angles, there are substantial differences between the contributions of non-uniformities to the energy resolutions measured with the scintillation and the Cherenkov signals. This difference is due to (irreducible) non-uniformities deriving from the impact-point dependence of the sampling fraction discussed in Section 5.1. As the angle increases, this effect rapidly vanishes (see, for example, also Fig. 10), and any remaining non-uniformities for angles $\theta > 2°$ are the result of (avoidable) effects, such as the ones

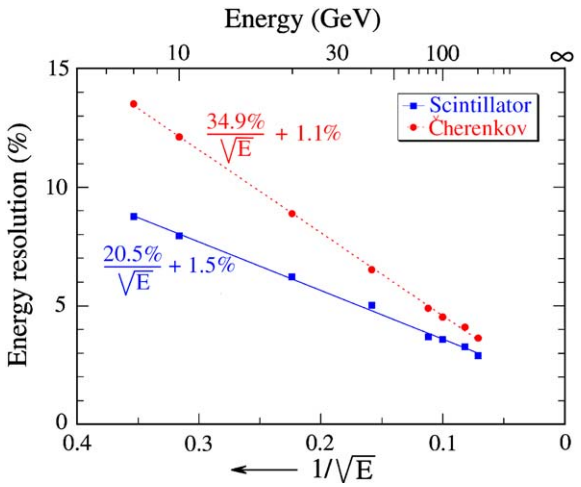

Fig. 20. The energy resolution as a function of energy, measured with the scintillating (squares) and Cherenkov fibers (circles), for electrons entering the calorimeter in the tilted position, B(3°, 2°).

discussed in Section 5.3. In that context, it is interesting to note that the remaining constant term $B \approx 2\%$ is very similar to the signal variations observed in Fig. 18.

In Section 5.1, we saw that the effects of all non-uniformities could be eliminated, or at least greatly reduced, by selecting an event sample with the same impact points. In this way, for example, a Gaussian response function could be obtained (Fig. 13). We investigated if similar improvements could be achieved with regard

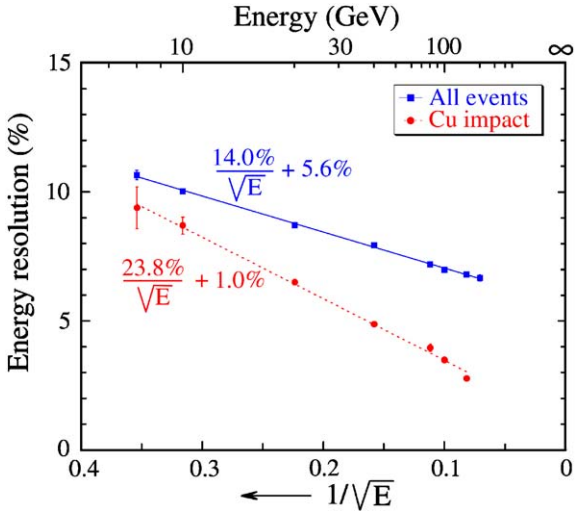

Fig. 21. The energy resolution as a function of energy, measured with the scintillating fibers for electrons entering the calorimeter in the untilted position, A(2°, 0.7°). The circles represent the results obtained for an event sample in which the electrons entered the calorimeter in the copper located in between horizontal fiber layers, the squares represent all data.

to the energy resolution. Some results of this study are shown in Fig. 21, where the energy resolution as a function of energy is given for the scintillating fiber signals. Data from a subsample of events in which the electrons entered the DREAM calorimeter in the copper plane in between horizontal fiber planes are compared with those from the entire event sample. Fits to Eq. (1) show that the constant term is reduced from 5.6% for all events to 1.0% in the copper subsample. Especially at the highest energies, the resolution is significantly better in such a subsample. At low energies, the differences are less significant. This is due to the fact that at low energy, the resolution is increasingly dominated by the stochastic term. Also, the correlation between the hodoscope coordinates and the impact point of the particles in the DREAM calorimeter (and thus the purity of the subsample) is not as good as at high energies, as a result of dispersion in the beam and multiple scattering in the material between the hodoscope and the calorimeter.

5.5. Light yield and sampling fluctuations

After having analyzed the contributions of response non-uniformities to the em energy resolution, which cause deviations from $E^{-1/2}$ scaling, we now turn to the factors that are responsible for the $E^{-1/2}$ term itself: photoelectron statistics and sampling fluctuations. The following analysis was carried out for the central calorimeter tower, where the Cherenkov signals were generated by quartz (Q) fibers. By comparing the results obtained with the two different active media, it is possible to disentangle the various contributions, as follows. The parameters A can be decomposed into contributions from fluctuations in the number of photoelectrons contributing to the signals ($A_{\text{p.e.}}$) and sampling fluctuations (A_{samp}):

$$A(\text{S}) = A_{\text{samp}}(\text{S}) \oplus A_{\text{p.e.}}(\text{S})$$
$$A(\text{Q}) = A_{\text{samp}}(\text{Q}) \oplus A_{\text{p.e.}}(\text{Q}). \quad (3)$$

Based on the measured gain/voltage characteristics of the PMTs and on the voltages at which the PMTs were operated to achieve the desired number of ADC counts per GeV, we measured the gain of the Cherenkov PMTs to be a factor of 4.1 higher than that of the scintillator PMTs, for the same number of ADC counts per GeV. Therefore, $A^2_{\text{p.e.}}(\text{Q}) = 4.1 A^2_{\text{p.e.}}(\text{S})$.

Since both types of fibers have the same cross section and are located in the same holes, their contributions to the sampling fluctuations are related as [1]:

$$A_{\text{samp}}(\text{S}) = \sqrt{\frac{4}{3}} A_{\text{samp}}(\text{Q}) \quad (4)$$

given that each copper tube contains four Cherenkov fibers and three scintillating fibers (see Fig. 1).

Based on these considerations and on the measured values of A(S) (24%) and A(Q) (38%), we could determine all individual contributions to the em energy resolution. Sampling fluctuations and photoelectron statistics contributed about equally to the resolution for the scintillator readout: $16.6\%/\sqrt{E}$ and $17.3\%/\sqrt{E}$, respectively. The resolution for the Cherenkov readout was dominated by fluctuations in the relatively small

number of photoelectrons: $35\%/\sqrt{E}$. The contribution from sampling fluctuations was $14.3\%/\sqrt{E}$ in this case.

Since the light yield (L) of the detector, i.e. the number of photoelectrons generated per GeV of deposited energy, is related to $A_{\text{p.e.}}$ as

$$L = \frac{1}{A^2_{\text{p.e.}}} \tag{5}$$

we found that the detector generated, on average, 8 photoelectrons per GeV in the (quartz) Cherenkov channel and 33 photoelectrons per GeV in the scintillator channel.

5.6. Comparison of quartz and plastic Cherenkov fibers

Twelve of the 19 calorimeter towers, i.e. those constituting the outer ring, were equipped with plastic Cherenkov fibers, instead of the quartz fibers that were used in the inner region of the detector. These plastic fibers were a factor of 20 cheaper. If only for that reason, it was interesting to investigate to what extent the performance would be affected should these be used instead of quartz, for the entire detector.

One aspect of the performance is the light attenuation length. In that sense, the plastic fibers were somewhat worse than quartz: λ_{att} was measured to be 8 m, compared to 15 m for quartz[9]. However, the attenuation length is still considerably larger than that of the scintillating fibers ($\lambda_{\text{att}} = 5$ m) and is adequate for this type of detector. Other, more crucial performance aspects concern the light yield and, most importantly, the possible generation of scintillation light.

We investigated these issues with 40 GeV electron data collected from all 19 calorimeter towers, taken in the untilted position, A(2°, 0.7°). In this position, the differences between the scintillation and Cherenkov signals are most striking (see, for example, Fig. 7) and, therefore, this is the best position to study the eventual presence of a scintillating component in the light generated by the plastic fibers. The χ^2 value of the Gaussian fit is a very sensitive indicator of contamination by scintillating agents. Since the scintillation photons in the scintillating fibers outnumber the Cherenkov photons by a large factor, even a minuscule contamination of the plastic fibers would reveal itself through the shape of the response function. The reduced χ^2 of a Gaussian fit to the 40 GeV electron signals from the scintillating fibers in this geometry was found to be $\chi^2/N_{\text{dof}} = 66$, versus 4.5 for the Cherenkov signals (see Fig. 7).

Fig. 22b shows the reduced χ^2 value of a Gaussian fit to the signal distribution for each of the 12 calorimeter towers that were equipped with plastic fibers. The χ^2/N_{dof} distribution for these 12 towers has a mean value of 4.9 and an rms spread of 2.7. This is compatible with the values found for the seven towers equipped with quartz fibers ($\chi^2/N_{\text{dof}} = 7.2 \pm 3.3$), and much

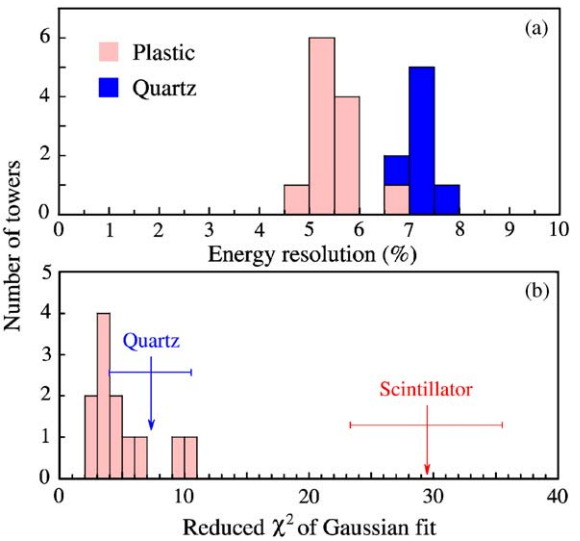

Fig. 22. Distribution of the fractional energy resolution, σ_{Gauss}/mean (a), and of the reduced χ^2 of the Gaussian fits to the 12 signal distributions (b), for 40 GeV electrons steered into each of the 12 DREAM towers equipped with clear plastic fibers. The resolutions for the Cherenkov signals from the seven towers in the central region that were equipped with quartz fibers are shown as well. The arrows in panel *b* indicate the average reduced χ^2 values obtained for pure Cherenkov (quartz) and pure scintillating media. The rms spread around these average values is indicated by a horizontal bar.

[9]These comparative attenuation measurements were carried out with radioactive sources at an optical bench. The results were consistent with those obtained with em showers.

smaller than the values typically found for the scintillating fibers. Therefore, we conclude that the signals from the plastic fibers are entirely due to Cherenkov light.

In Fig. 22a, the energy resolutions for the Cherenkov signals from the 19 calorimeter towers are given. Each entry represents the fractional width of the signal distribution for the tower into which the 40 GeV electron beam was steered. These resolutions are slightly worse than those for the sum of all towers, because of the contributions of lateral leakage fluctuations that play a role when we consider only the signals from the hit tower. For example, the resolution for the central tower is 7.15%, instead of 6.83% for the sum of all towers.

The figure reveals a significant difference between the energy resolution obtained with the quartz fibers and with the plastic fibers. The latter was found to be *better*: $5.51\% \pm 0.49\%$ (plastic) vs. $7.15\% \pm 0.23\%$ (quartz). Since the contributions of sampling fluctuations ($14.3\%/\sqrt{E}$, see Section 5.5) and of deviations from $E^{-1/2}$ scaling should be the same in both cases, this difference must be entirely due to a difference in light yield. After subtracting the contributions from these other effects in quadrature from the measured resolution, we found that photoelectron statistics accounted for fluctuations with a σ/E of 3.85% ($23.5\%/\sqrt{E}$) and that the Cherenkov light yield of these plastic fibers thus amounted to 18 photoelectrons per GeV, compared to 8 p.e./GeV for quartz.

This difference is commensurate with expectations on the basis of differences in light attenuation and in the numerical aperture of the fibers. The numerical aperture of the quartz fibers was 0.33, vs. 0.50 for the plastic fibers. The light yield is proportional to the numerical aperture squared, which means that we may expect 2.3 times more Cherenkov photons from the plastic fibers than from the quartz ones. Light attenuation in the 2.5 m long fibers reduces this number by a factor $\exp(-2.5/8)/\exp(-2.5/15) = 0.86$, so that we expect twice as many Cherenkov photoelectrons from the plastic fibers, as compared with the quartz fibers, in agreement with the above-mentioned results (18 vs. 8 p.e./GeV).

5.7. Angular dependence of Cherenkov signals

Contrary to the scintillator response, the Cherenkov response of a fiber calorimeter depends on the angle of incidence of the electrons. When quartz-fiber calorimeters were first built, some believed that these devices would only work when oriented at an angle close to the Cherenkov angle ($\sim 46^\circ$) with respect to the incoming particles. However, it turned out that also at other orientations useful signals can be obtained. In particular at an angle close to 0°, which is crucial for operation in a colliding-beam environment. The response is about half of the maximum possible value which, not surprisingly, is reached at 46° [9].

In these tests, we obtained experimental data for a number of different angles between the shower axis and the fiber direction : 2°, 6° and 24°. At each angle, the scintillator response provided a useful and precise reference point, since the scintillator response does *not* depend on the angle of incidence of the particles. Fig. 23 shows the Cherenkov

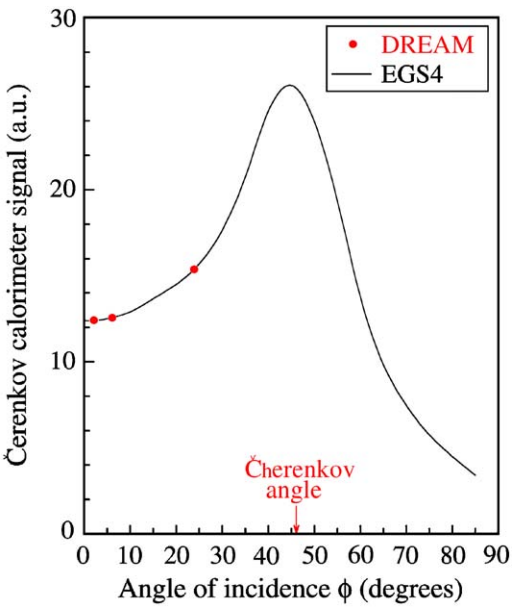

Fig. 23. The Cherenkov signal of the DREAM calorimeter for 40 GeV electrons, as a function of the angle of incidence of the particles. The angle-independent scintillator response was used for normalization purposes. The curve represents the results of EGS4 Monte Carlo simulations.

signal of the DREAM calorimeter, as a function of the angle of incidence of the electrons. The 40 GeV electron beam was used at all angles. The figure also shows the results of Monte Carlo simulations, taken from [9]. Our measurements show that the response at 24°, the largest angle at which we performed measurements, is about 26% larger than that at the smallest angle (2°). These results are in good agreement with the Monte Carlo predictions.

6. Conclusions

We have tested the electromagnetic performance of a novel type of sampling calorimeter, equipped with two independent active media, scintillating fibers (for the measurement of the energy deposit dE/dx) and fibers measuring the production of Cherenkov light in the showers. This calorimeter was designed for the detection of hadrons and jets. The em performance is very sensitive to the angle of incidence of the particles relative to the fiber direction. When this angle is smaller than $\sim 3^\circ$, the calorimeter response depends on the impact point of the particles. This has consequences for several aspects of the performance, most notably the em energy resolution and the signal linearity. The effects are considerably smaller for the Cherenkov signals than for the scintillator signals.

The em energy resolution of this instrument was measured to scale as $24\%/\sqrt{E}$ for the scintillator signals and as $38\%/\sqrt{E}$ for the Cherenkov signals. Deviations from such scaling were only significant for angles smaller than 3°, and only for the signals from the scintillating fibers. We measured the contributions of sampling fluctuations and photoelectron statistics to the $E^{-1/2}$ term. For the scintillator signals these two contributions were about equal at $\sim 17\%/\sqrt{E}$. The Cherenkov resolution in quartz was dominated by fluctuations in the number of photoelectrons ($\sim 35\%/\sqrt{E}$), while sampling fluctuations contributed $14\%/\sqrt{E}$. The Cherenkov light yield was measured to be 18 photoelectrons per GeV in the clear plastic fibers, compared to 8 for the quartz fibers. This difference is mainly a consequence of the larger numerical aperture of the plastic fibers.

The response of the detector to electrons was found to be reasonably uniform. Response fluctuations resulting from non-uniformities in the photocathode surface and from variations in fiber properties were $\sim 2\%$ for the scintillator signals and $\sim 3\%$ for the Cherenkov ones. Boundary effects between calorimeter towers were insignificant. This detector was first and foremost developed for detecting hadrons and hadron jets. Since the number of fibers contributing to the signals from hadronic showers is much larger than that for the em showers studied here, the effects of the observed non-uniformities are correspondingly smaller and, therefore, in practice negligible. However, a dedicated em calorimeter of this type would have to improve in response uniformity (as well as in other aspects) in order to be compatible with other high-quality em calorimeters.

Acknowledgements

We gratefully acknowledge the contributions of Tracy McAskill, Vladimir Nagaslaev, Alan Sill, Veronica Stelmakh, Yunyong Wang, Erika Washington and Kim Zinsmeyer to the construction of the DREAM detector. We thank CERN for making particle beams of excellent quality available. Our beam tests would not have been possible without the help we received from Claude Ferrari and Maurice Haguenauer. We thank K. Kuroda for loaning us the fiber hodoscopes, and A. Gorin and I. Manouilov for their assistance with the data acquisition system. This study was carried out with financial support of the United States Department of Energy, under contract DE-FG02-95ER40938, and the Advanced Research Program of the State of Texas.

References

[1] R. Wigmans, Calorimetry—Energy Measurement in Particle Physics, International Series of Monographs on Physics, Vol. 107, Oxford University Press, Oxford, 2000.
[2] P. De Barbaro, et al., Nucl. Instr. and Meth. A 457 (2001) 75.

[3] N. Akchurin, et al., Hadron and Jet Detection with a Dual-Readout Calorimeter, Nucl. Instr. and Meth., accepted for publication.
[4] F.G. Hartjes, R. Wigmans, Nucl. Instr. and Meth. A 277 (1989) 379.
[5] V. Agoritsas, et al., Nucl. Phys. B (Proc. Suppl.) 44 (1995) 323.
[6] V. Agoritsas, et al., Nucl. Instr. and Meth. A 372 (1996) 63.
[7] N. Akchurin, R. Wigmans, Rev. Sci. Instr. 74 (2003) 2955.
[8] N. Akchurin, et al., Comparison of High-Energy Shower Profiles Measured with Scintillation and Cherenkov Light, Nucl. Instr. and Meth., accepted for publication.
[9] O. Ganel, R. Wigmans, Nucl. Instr. and Meth. A 365 (1995) 104.